DEUTSCHES ELEKTRONEN – SYNCHROTRON DESY

DESY 87-145
October 1987

JETS - FROM GeV TO TeV

by

G. Ingelman

Deutsches Elektronen-Synchrotron DESY, Hamburg

ISSN 0418-9833

NOTKESTRASSE 85 · 2 HAMBURG 52

To be sure that your preprints are promptly included in the
HIGH ENERGY PHYSICS INDEX,
send them to the following address (if possible by air mail):

DESY
Bibliothek
Notkestrasse 85
2 Hamburg 52
Germany

DESY 87-145
October 1987

ISSN 0418-9833

Jets — from GeV to TeV [1]

G. Ingelman
Deutsches Elektronen-Synchrotron DESY
Notkestrasse 85, D-2000 Hamburg 52, FRG

Abstract

The properties of jets at the present GeV energy scale is discussed in terms of perturbative QCD processes and non-perturbative hadronization models. Based on this framework, the expected jet characteristics at HERA and future accelerators in the TeV energy region are illustrated.

1 Introduction

The properties of high energy hadron jets are determined both by hard, or semihard, parton processes that can be calculated in perturbative QCD and by soft, i.e. low momentum transfer, hadronization processes which cannot be calculated from fundamental principles at present. Jet physics is therefore an important subject for both practical and theoretical reasons. The theoretical calculations of fundamental interactions at the quark level must be related to the experimentally observable world of hadrons in order to make detailed comparisons between theory and data. Moreover, in spite of the success of *perturbative* QCD we still lack a basic understanding of the hadronisation process. In fact, the confinement induced transition from perturbatively produced partons into final state hadrons is a major unsolved problem in high energy physics. Nevertheless, phenomenologically successfull models have been developed to describe the observations and systematize our experiences from different kinds of interactions. To the extent that these models are not just parametrizations of data, but rather based on more or less elaborate physical models, they can have a large predictive power leading to useful tests of the underlying assumptions of the models. Extrapolations to much higher energies is in this case also meaningful.

Jets may also serve as a tool for searching for new heavy objects that may be produced at future accelerators. Since many such states are expected to decay into jets, or jets and leptons, one would like to measure jets and treat them as 'particles', i.e. 4-vectors, in a search for resonances in the invariant mass combinations of jets. In order to judge how well this can made and what requirements the experimental equipment must meet, one needs detailed information on the properties of jets at the TeV energy scale. The flow of energy and particles within a jet is important for calorimetry and the possibilities to perform tracking in a jet environment to, e.g., measure special particles like leptons or photons.

Although a jet can theoretically be identified with a quark or gluon produced in a large momentum transfer process, it is in reality a matter of experimental definition. This is usually done based on the energy flow of hadrons in a calorimeter using some cone to define the angular width of the jet. Since a parton from a hard scattering tend to emit bremsstrahlung gluons (and quarks to a lesser extent) the experimental jet can be the result of more than one parton. One therefore needs a complete model that takes both perturbative parton emission and the subsequent hadronization into account so that experimentally realistic jet finding algorithms can be employed to predict useful information on jet properties.

2 Perturbative jet evolution

The calculation of matrix elements in perturbation theory of the electroweak and strong interactions is well defined, but quickly become very complicated for higher order processes in QCD. Therefore, only lowest order diagrams giving the leading and next-to-leading order processes can be calculated exactly so that only processes with a few final state partons can be treated in this way. In e^+e^- annihilation and high-$p_\perp$ hadron-hadron scattering exact matrix elements have been calculated up to order α_s^2 [1] and α_s^4 [2], respectively, both giving rise to at most four partons in the final state (spectators not counted). In deep inelastic scattering only order α_s matrix elements are available [3] giving two final partons in addition to the target remnant. For higher order diagrams, giving rise to multiparton final states, some approximation has to be made. Using analytical techniques, some effects arising from the emission of many but softer gluons can be obtained by a summation procedure based on the leading logarithm approximation, e.g. the energy-energy correlation in e^+e^- annihilation [4].

In another method the parton radiation processes is dynamically simulated, which has the advantage that complete final parton states can be generated such that any observable is in principle accessible. The basic idea is here that partons emitted in a large momentum process can be off their mass shell and will therefore emit bremsstrahlung. For simplicity we consider the case of e^+e^- annihilation at a momentum transfer Q^2 where the two emerging partons can be off shell up to $\mathcal{O}(Q)$ and therefore cascade into a shower of partons as illustrated in Fig. 1. Such parton cascade models has been developed to a high degree over the last few years [5,6,7]. The common feature is that first order QCD matrix elements in the leading logarithm approximation is used for each separate branching. Provided that the offshellness of the partons are strongly ordered, i.e. $m_1^2 \gg m_2^2 \gg m_3^2$ etc in Fig. 1, the cross section for the whole process factorises into a product of the probabilities for each separate branching. This results in an iterative process, suitable for Monte Carlo simulation techniques, which is stopped when all parton virtualities, i.e. m_i^2, are below a chose cutoff, t_{cut}. Together with Λ_{QCD} this cutoff regulates the amount of partons radiated.

[1] Invited talk at the XVth International Winter Meeting on Fundamental Physics, Sevilla, Spain, 23-27 February 1987.

One should bear in mind that this approximation is not expected to work properly for hard gluon emission at large angles where interferences between diagrams where the gluon is emitted from different parton lines are important. These models are rather intended for studies of e.g. jet broadening due to the emission of several but not very hard gluons at large angles. Nevertheless, these models may be used also for multiple jet phenomena simply because better higher order calculations are lacking at present; the general features will certainly be adequately described although the rates and some distributions will not be exactly the correct ones.

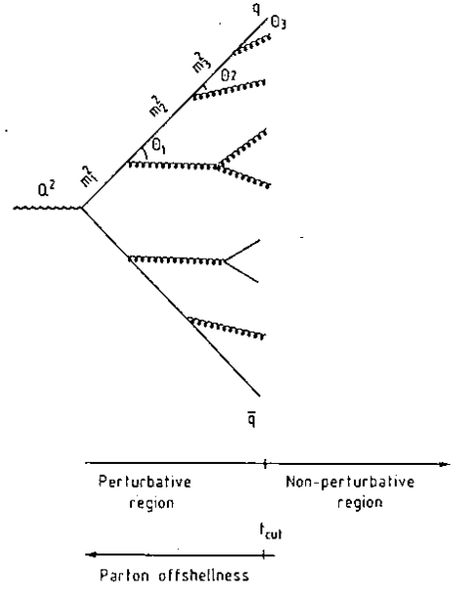

Figure 1: *Schematic representation of a parton cascade evolution from a quark-antiquark pair produced at a given Q^2, e.g. in e^+e^- anihilation.*

An interesting sophistication of this kind of model is that interference between soft gluons can be taken into account by imposing an angular ordering in the emission [6], i.e. $\theta_1 > \theta_2 > \theta_3$ etc in Fig. 1. Since this interference is destructive, fewer soft partons will be emitted (for a given t_{cut}), which can be intuitively understood as follows. A soft gluon, having a larger wavelength, cannot resolve the individual colour charges in the cascade, which therefore act coherently as a single colour charge for soft gluon emission. This strict angular ordering also takes some next-to-leading corrections effectively into account [8]. In the following the basic formalism of parton cascades will be illustrated, but for a more complete treatment we refer to [5,6,7].

The final state radiation is timelike, i.e. all partons have $m^2 \geq 0$, and is based on the iterative use of the parton braching as given by the Altarelli-Parisi equations [9]

$$dP_{a\to bc} = \frac{\alpha_s(Q^2)}{2\pi}\,\frac{dm_a^2}{m_a^2}\,P_{a\to bc}(z)\,dz \tag{1}$$

where Q^2 is a function of the virtuality m_a^2 of the 'mother' parton, a, the $p_\perp$ in the branching and z, which gives the sharing of energy (or more generally some function of energy and momentum) between the 'daughters' b and c. The functions $P(z)$ are the splitting kernels given by

$$P_{q\to qg}(z) = \frac{4}{3}\,\frac{1+z^2}{1-z} \tag{2}$$

$$P_{g\to gg}(z) = 6\,\frac{[1-z(1-z)]^2}{z(1-z)} \tag{3}$$

$$P_{g\to q\bar{q}}(z) = \frac{1}{2}\,[z^2+(1-z)^2] \tag{4}$$

The probabitity that a parton does *not* branch is then obtained by exponentiation of eq. (1) giving the Sudakov form factor

$$S_a(m^2) = exp\left\{-\int_{t_{cut}}^{m^2}\frac{dm'^2}{m'^2}\int_{z_-(m')}^{z_+(m')}dz\,\frac{\alpha_s(Q^2)}{2\pi}\,P_{a\to bc}(z)\right\} \tag{5}$$

where m^2 is given by Q^2 for the first branching and in later ones by m^2 in the previous branching. The probability distribution of the parton virtuality is then

$$P_a(m_{max}^2, m^2)\,dm^2 = S_a(m_{max}^2)\,\frac{d}{dm^2}\,\frac{1}{S_a(m^2)}\,dm^2 \tag{6}$$

and parton branches are generated by solving for m^2 in

$$S_a(m^2) = \frac{S_a(m_{max}^2)}{R} \tag{7}$$

where R is a random number in]0,1[. The process is iterated until all parton virtualities are smaller than t_{cut} at which point they are put on shell.

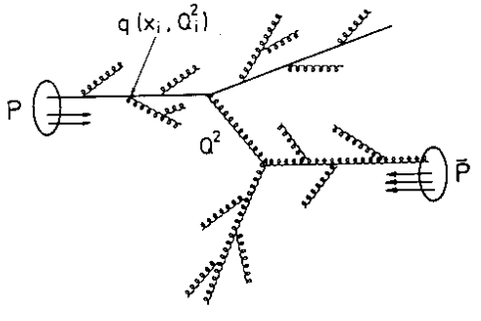

Figure 2: *Initial and final state parton radiation in high-$p_\perp$ hadron-hadron scattering, e.g. $p\bar{p}$ collisions.*

In high-$p_\perp$ hadron-hadron collisions, not only the final scattered partons can emit gluon radiation, but also the partons entering into the hard scattering, Fig. 2. In this case, the

radiating parton developes a negative virtuality, i.e. has a space-like 4-vector giving $m^2 < 0$. This initial state cascade evolution may be viewed as a quantum fluctuation which can only be realized in a large momentum transfer process which put the parton back on shell or to a positive virtuality, i.e. $m_i^2 < 0 \rightsquigarrow m_f^2 \geq 0$. For practical reasons it is better to start with the hard scattering, given by the $2 \rightarrow 2$ exact matrix elements, and perform the parton cascade evolution backwards in time. Such a scheme, developed in [10], must also take constraints from the structure functions into account, since at each intermediate step one should have the correct probability of finding a parton with momentum fraction x_i at the given momentum transfer scale Q_i^2 as indicated in Fig. 2. This leads to a modified splitting equation

$$dP_b = |dt| \, \frac{\alpha_s(Q^2)}{2\pi} \sum_a \int \frac{dx'}{x'} \, \frac{f_a(x',t)}{f_b(x,t)} \, P_{a \rightarrow bc}\left(\frac{x}{x'}\right) \tag{8}$$

and a modified form factor

$$S_b(x, t_{max}, t) = exp\left\{ - \int_t^{t_{max}} \frac{dt'}{t'} \, \frac{\alpha_s(Q^2)}{2\pi} \sum_a \int \frac{dx'}{x'} \, \frac{f_a(x',t')}{f_b(x,t')} \, P_{a \rightarrow bc}\left(\frac{x}{x'}\right) \right\} \tag{9}$$

for the probability that a parton b remains at x from t_{max} to t. Otherwise the procedure is similar to that of final state radiation. The structure functions, f_a, has the effect of reducing the amount of radiation as compared to the case for final state radiation. For the properties of high-$p_\perp$ jets the initial state radiation is of less importance and we will not pay much attention to it in the following. It does, however, influence the underlying event and also generate a transverse momentum of the hard scattering system. The $p_\perp$ of a jet-jet system or a W can thus be described by this effect [11].

Although these parton shower algorithms are phenomenologically very useful, one should realize their limitations. Not only do they involve the QCD leading log approximation, but also some ingredients which are not theoretically well-defined, like the definition of the z and Q^2 variables. Therefore, they cannot replace exact matrix element calculations for fundamental tests of QCD and the determination of Λ_{QCD} in a well-defined renormalization scheme.

Since α_s used in each separate branching depends on the momentum transfer in that vertex, it gets larger the further the cascade is evolved and the perturbative approximation will then break down at some point when the parton virtualities become small. The parameter t_{cut} determines the border line between the region where perturbative QCD can be considered trustworthy and the following non-perturbative region, Fig. 1. There is no theoretical motivation for the choice of a particular t_{cut}-value, it is more related to ones confidence in the perturbative QCD shower approach and the method used for the final hadronization step. It is therefore desirable that the complete model is stable against variations of this parameter.

3 Non-perturbative hadronization

The simplest fragmentation model is to let all partons from the shower hadronize independently of each other using, e.g., the Field-Feynman parametrization [12]. This leads, however, to a significant dependence on t_{cut} [13], since the additional soft gluons obtained by a lower

cutoff result in an increasingly soft hadron spectrum and correspondingly increasing multiplicity. Monte Carlo models that employ this scheme are forced to have a rather large parton shower cutoff in order to reproduce basic features of the data, but then loose effects of multiple soft gluon emission.

Physically more interesting is the possibility of cluster formation from the partons and, in particular, the idea of preconfinement [14]. Given the well-defined colour ordering of the planar graph the partons can be associated to colour singlet clusters (Fig. 3a) which could form a link to the hadronic final state. Considering e^+e^- annihilation for simplicity, the original $q\bar{q}$ colour singlet system can give rise to more than one cluster only if additional $q\bar{q}$ pairs are formed in the perturbative shower evolution. Consequently, the cluster multiplicity and mass spectrum depends on the frequency of the $g \rightarrow q\bar{q}$ branching. Analytical calculations in an asymptotic limit indicates that the typical cluster mass is close to the shower cutoff, i.e. close to the hadronic mass scale, and, moreover, essentially independent of Q^2 [14]. More detailed investigations based on Monte Carlo simulations show that this is not quite correct [15]. The mass spectrum of such clusters, Fig. 3b, has indeed a peak at small masses, but also a long tail to large masses which makes the average mass quite appreciable and also increasing with increasing Q^2, Fig. 3c. The cluster masses are therefore in reality significantly above the hadron mass scale and become even more so at higher energy scales. Unfortunately, this prevents an easy connection between perturbatively produced clusters and the final state hadrons.

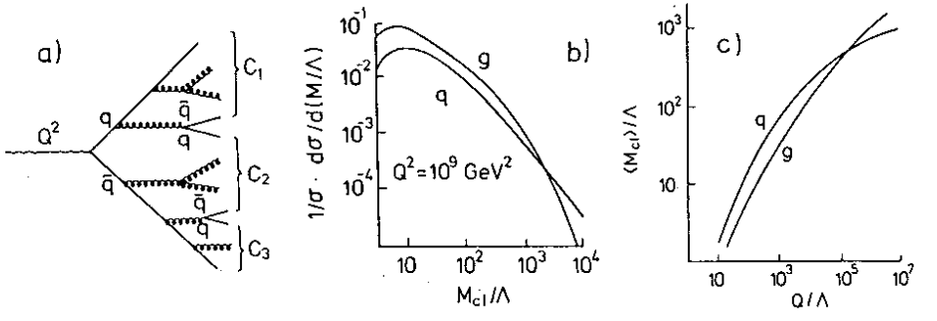

Figure 3: *(a) Preconfinement of perturbatively produced quanta into colour singlet clusters. (b) Cluster mass distribution at asymtotic energy. (c) Average mass versus energy scale. Energies and masses are scaled with Λ_{QCD}; q and g refer to quark and gluon jet, respectively. From [15].*

Nevertheless, it is possible to construct phenomenological cluster models [6] by first splitting the gluons into $q\bar{q}$ pairs and then let colour-connected $q\bar{q}$ pairs form lower mass clusters, which are finally decayed into ordinary hadrons (including resonances) using pure phase space. The continous cluster mass spectrum obtained will obviously depend on the parton shower cutoff value and hence a low cutoff is preferable in order to get cluster masses not too much above the hadron mass scale. Even with a small cutoff, however, large mass clusters will occur and their isotropic phase space decay will produce too spherical events compared to e^+e^- data. This is usually solved by splitting heavy clusters, with a mass larger than 3-4

GeV, into lower mass clusters using a longitudinal decay. Another potential problem with this method is that the particle composition may change with the cutoff value since with a lower t_{cut} the cluster masses will become smaller and the rate of heavier particles, like baryons, may be reduced because of the reduced phase space available.

Another approach is to connect the perturbatively produced partons, whose colour ordering is given by the shower evolution, with a colour string force field and apply the Lund fragmentation model [16] for the final hadronization step. A colour triplet and antitriplet charge, e.g. q and $\bar{q}$, are here represented by the endpoints and a gluon colour octet charge by an energy-momentum carrying kink on the string, Fig. 5a. Thus, a rather complicated string topology arise when many gluons have been emitted, which requires technical improvements of the model [17]. As discussed in [13,18], the string model provides the desired stability of the final hadron state properties with respect to variations of the arbitrary t_{cut} parameter since the extra gluons emitted with a lower cutoff will only produce small disturbances on the string configuration obtained without them. In e^+e^-, e.g., more than one colour string system will only occur if $q\bar{q}$ pairs have been produced in the perturbative evolution; these strings thus correspond to the 'preconfinement clusters' in Fig. 3a.

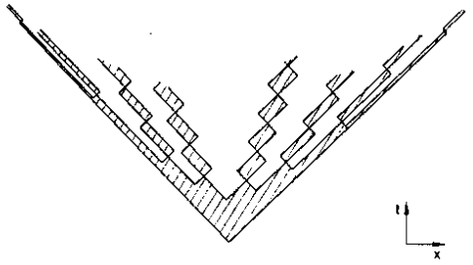

Figure 4: *Space-time picture of a separating quark and antiquark with intermediate colour string field (hatched) which breaks by $q\bar{q}$ creation leading to meson production.*

The QCD force field between two colour charges is believed to form a flux tube with limited transverse size of the order of a hadron diameter. This different character as compared to the dipole field between electric charges is attributed to the self-interactions among the colour charged gluons that are the quanta of the field. Although this is not strictly proven, it is supported by non-perturbative lattice calculations (see [19] and references therein). The dynamics of this essentially one-dimensional field is in the Lund model approximated by that of the massless relativistic string, which is a relativistically invariant and causal generalisation of a one-dimensional constant force field. The constant κ in the linearly rising potential $V(r) = \kappa r$, is the string tension which is estimated to be $\simeq 1$ GeV/fm, or in metric units 16 tons/m! The kinetic energy of the separating colour charges, e.g. the quark and antiquark produced in e^+e^- annihilation, is thus transfered into potential energy which can be lowered by the production of new $q\bar{q}$ pairs in such a way that the colour field is screened and the string broken up into smaller parts, Fig. 4. The $q\bar{q}$ pair creation probability can be calculated as a tunneling process giving

$$P \sim e^{-\frac{\pi}{\kappa}m_q^2}\, e^{-\frac{\pi}{\kappa}p_\perp^2} \qquad (10)$$

which expresses the price in terms of field energy that has to be payed to produce the transverse mass of the $q\bar{q}$ pair. This results in a suppression of heavier flavours, $u\bar{u} : d\bar{d} : s\bar{s} : c\bar{c} = 1 : 1 : 0.3 : 10^{-11}$, and a Gaussian transverse momentum spectrum with $< p_\perp >= 0.3 - 0.4$ GeV of the final hadrons (w.r.t. the string); in agreement with experimental findings. Thus, the string is broken by a $q\bar{q}$ pair production and a meson is formed with a 'nearby' q or $\bar{q}$, leaving a reduced jet system and the procedure is iterated until the total available energy has been transformed into mesons, Fig. 4. Also baryons are produced through the effective production of diquark-antidiquark pairs in the string breaking, either directly in a simple model or trough stepwise $q\bar{q}$ production in a more elaborate model based on quantum fluctuations in the colour field [20].

The energy-momentum fraction, z, that a hadron takes from the total available in each step is given by a 'splitting' function, $f(z)$, which is deduced from a symmetry condition, namely that it should not matter whether the string is being 'cut into mesons' from one side or the other. This results in an essentially unique splitting function [21,16]

$$f(z) = \frac{(1-z)^a}{z}\, exp\left\{-\frac{bm_\perp^2}{z}\right\} \qquad (11)$$

where the parameters a and b are related to the only two important features (regarding the longitudinal structure) of this kind of iterative fragmentation model, namely the total multiplicity or the height of the central rapidity plateau and the strenght of the rapidity correlation between nearby particles in the fragmentation chain. By uniqueness of eq. (11) is meant that if the hadronization process is essentially of a classical stochastic nature as assumed, then this is the only form which has this symmetry property, whereas this need not be the case if quantum corrections are important. Hence the testing of eq. (11) probes fundamental properties of the hadronization process. An important phenomenlogical consequence of this function is that heavy particles, or more generally hadrons with a large transverse mass $m_\perp$, will have a harder fragmentation spectrum; as is also observed to be the case for charm and bottom mesons.

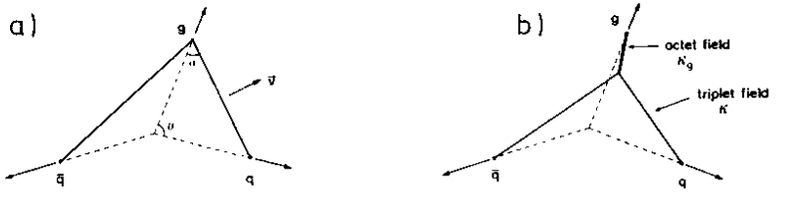

Figure 5: *(a) Representation of a $q\bar{q}g$ system using a triplet string stretched via the colour octet gluon. The velocity of a string piece is $v = \cos\theta/2$. (b) Alternative gluon model with a colour octet string joining the two triplet strings at a junction.*

Representing a gluon with a kink, Fig. 5a, means that no additional assumptions and parameters are needed for the gluon fragmentation model, since it is determined by the basic break-up of the colour triplet field as given by quark jets and constrained by, e.g., e^+e^- data. The two strings stretched from the gluon imply a considerably softer fragmentation

of a gluon jet as compared to that obtained from the single string quark jet. Gluon jet fragmentation is, however, experimentally not well measured and other models can certainly be conceived of. One possibility [22], which can be included in the string framework, is that the gluon stretches a colour octet field which is split into two triplet fields at a junction, Fig. 5b. The position of the junction is determined by the ratio κ_g/κ_q of the string tensions in the octet and triplet fields and if it is larger than two, as suggested by the relevant Casimir operator eigenvalues in QCD, it is energetically favourable for the octet field to collapse to zero length; thus giving the gluon as a kink on the string. The hadronization of an octet field is, furthermore, unknown and additional assumptions would have to be made to construct a model. On general grounds one would expect an octet field to break by gluon pair creation resulting in the production of glueballs (if existing) and isoscalar particles, but such a model [23] has been found inconsistent with results on η and ϕ production in Υ decays, whereas the Lund gluon-kink model does provide a good description [24].

Both the string and the cluster hadronization models are well tuned to describe present data, in particular from PETRA/PEP, and give therefore very similar results, although characteristic differences occurs in some particular observables. For the results discussed below, both at present energies and at the TeV energy scale, the two models give surprisingly good agreement and only string model results will therefore be given.

4 Jet properties at present energies

The importance of the higher order QCD effects included in the parton shower approach has been shown in e^+e^- annihilation at PETRA by the JADE collaboration [25]. Using a cluster algorithm to find jets, an excess of 4-jet events is observed as compared to the expectations from fixed order, but exact matrix elements up to order α_s^2. This deficiency cannot be cured by an increased α_s since the 3-jet rate will then be overestimated. The parton shower model can, however, reproduce the jet rates observed in the data, Fig. 6a, as well as the acoplanarity distribution, Fig. 6b, where the tail of more more spherical events is properly generated by the additional gluon radiation compared to the $\mathcal{O}(\alpha_s^2)$ model, which fails in this region.

The properties of high-$p_\perp$ jets in pp and $p\bar{p}$ collisions are also influenced by parton radiation processes. Thus, the jets measured by the UA1 collaboration [26] show clear evidence for these effects [27] in, e.g., the inclusive fragmentation function

$$D(z) = \frac{1}{N_{jet}} \cdot \frac{dN_{ch}}{dz} \quad ; \quad z = \frac{\vec{p}_{track} \cdot \vec{p}_{jet}}{|\vec{p}_{jet}|^2} \tag{12}$$

of charged particles. This is shown in Fig. 7 together with ISR data from the AFS collaboration [28] for comparison. The reason for the collider jets to be considerably softer is two-fold. Firstly, they are dominated by the intrinsically softer gluon jets, $\approx 60\%$ according to the model, whereas the ISR jet sample contains $\approx 70\%$ quark jets. Secondly, the harder interaction at the collider, resulting in $< p_{\perp jet} > \approx 39$ GeV compared to 13 GeV at the ISR, leads to more parton radiation; an effect which is also more accentuated by the colour octet charge of a gluon jet. The parton radiation also generate significantly enhanced transverse momenta with respect to the jet axis as seen in Fig. 8a. The low-$p_\perp$ part of the distribution

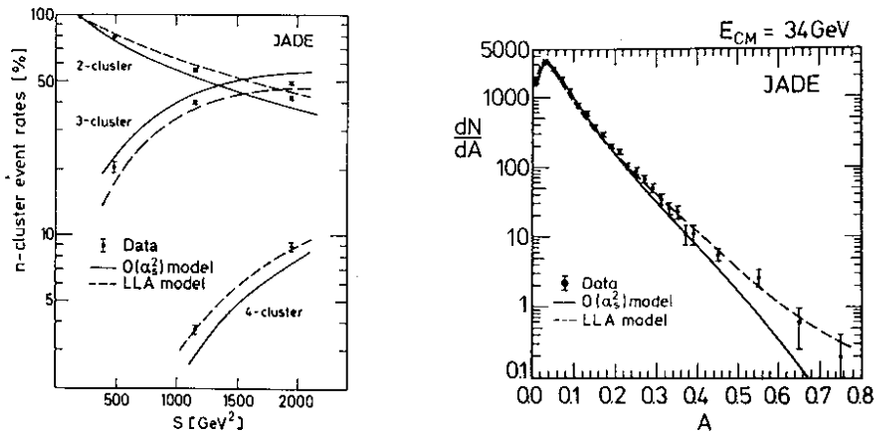

Figure 6: *n-jet event rates versus cms energy and acoplanarity distribution in e^+e^- data compared to model calculations [25].*

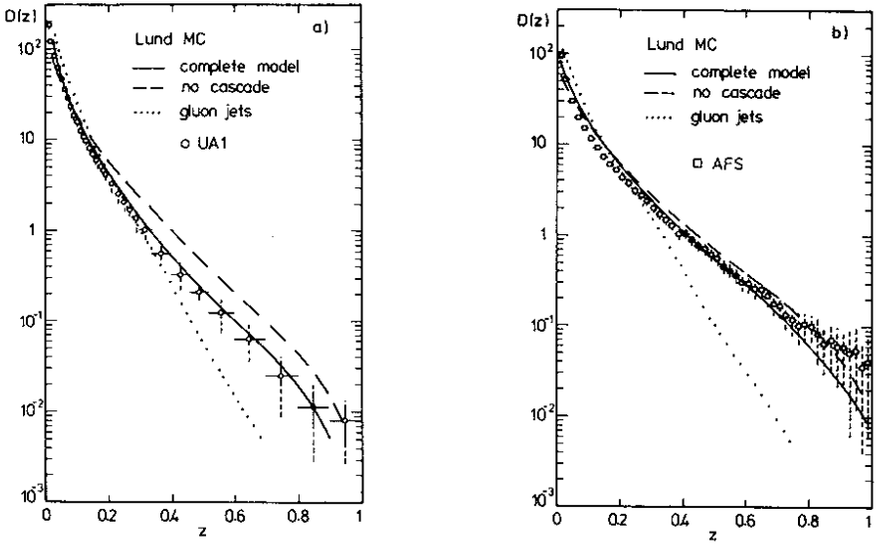

Figure 7: *Fragmentation functions, eq. (12), of high-$p_\perp$ jets at SPS collider (a) and ISR (b) energies. Data from UA1 [26] and AFS [28] collaborations with statistical (full) and systematic (dashed) error bars. The curves represent the model with the parton cascade included (full) and excluded (dashed), with quark and gluon jets mixed according to their relative cross-sections. Pure gluon jets including cascade are also shown (dotted curve) for comparison.*

depends rather sensitively on the cut applied to remove soft particles from the underlying event as illustrated with the two z-cuts shown for the data. Therefore, a mismatch between data and model calculation for the effective z-cut used may cause the observed difference at low $p_\perp$. The width of a jet, e.g. defined in terms of the energy flow versus rapidity around the jet axis as shown in Fig. 8b, can be rather well described with the inclusion of the final state parton radiation model, whereas without it a much too narrow jet is obtained with non-perturbative fragmentation alone. Although the rapidity distribution away from the jet, $|\eta| \gtrsim 1$, is considerably raised by the initial state parton radiation this is not sufficient to describe the observed energy flow plateau in Fig. 8b. This shows that the underlying event contains more physics than parton shower evolution and simple fragmentation.

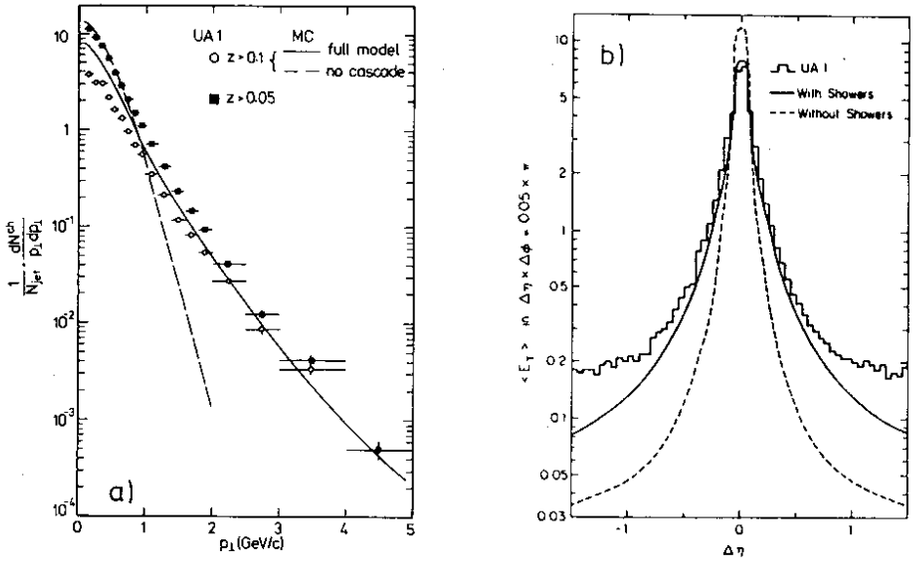

Figure 8: *(a) Transverse momentum distribution of charged particles with respect to the jet axis [27]. (b) Transverse energy flow of high-$p_\perp$ jets versus the rapidity distance to the jet axis [10]. Model curves including (full) and excluding (dashed) parton radiation (in (a) only final state emission).*

In [27] the properties of quark and gluon jets are investigated and a fair agreement between data and model is found. As expected, gluon jets are softer and wider than quark jets, Fig. 9a. There are, however, some tendency of a smaller quark-gluon difference in the data as compared the model. This could indicate an inadequacy of the model, but since they could also follow from a non-complete separation of quark and gluon jets or other systematic uncertainties in the data the model can be considered satisfactory. The variation with the momentum transfer Q^2 of the longitudinal and transverse jet properties are also found to be essentially the same in data and model, Fig. 9b. In the limited range covered by the UA1 data, the the Q^2 variation is rather small as expected from the dominant leading log Q^2 dependence in QCD.

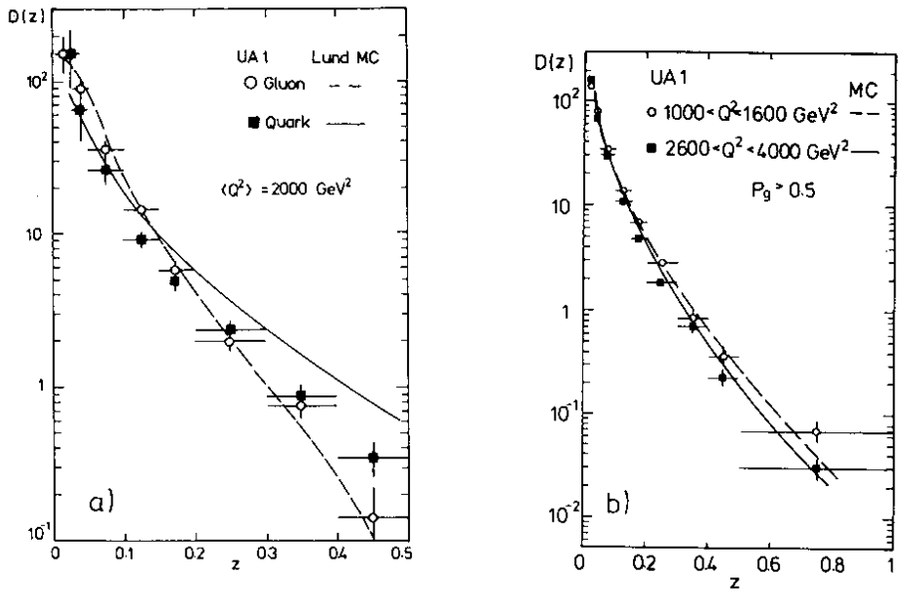

Figure 9: *(a) Fragmentation function for separated quark and gluon jet samples in data compared to pure quark and gluon model predictions. (b) Fragmentation function for gluon enriched jet samples at different Q^2 scales showing scaling violations in data and model.*

Current state-of-the-art models for the perturbative jet evolution and the non-perturbative fragmentation, either in terms of strings or clusters, are thus able to reproduce present-day data on jets quite well.

5 Jets at HERA

In deep inelastic lepton-nucleon scattering [29], the leading order quark parton model (QPM) process gives rise to two hadronic jets; the quark scattered by the exchanged vector boson and the target remnant spectator jet. In first order QCD an additional jet can be produced by hard gluon emission from the struck quark or, alternatively, through the boson-gluon fusion process into a quark-antiquark pair. At SPS/FNAL fixed target energies a model [30,31] based on these ingredients can successfully describe the experimental observations. In particular the European Muon Collaboration (EMC) has shown clear QCD effects in terms of transverse momentum properties and also evidence for the occurence of additional jets from gluon radiation [32]. The much higher energies that will be available through *ep* collisions at HERA will make higher order QCD corrections important [33]. These can be taken into account through the parton shower models by letting the struck quark radiate before and after it couples to the virtual boson. Although this is very similar to the initial and final state emission in high-$p_\perp$ scattering discussed above, there are technical differences in the algorithms [34]. It is also ambigous whether Q^2 or W^2 sets the scale for the maximum

virtuality in the shower, but W^2 seem to be the prefered choice [33,34]. Jets at HERA will be produced at an energy scale not very much larger than that presently studied in e^+e^- and $p\bar{p}$ colliders so that only modest, and therefore more reliable, extrapolations have to be made.

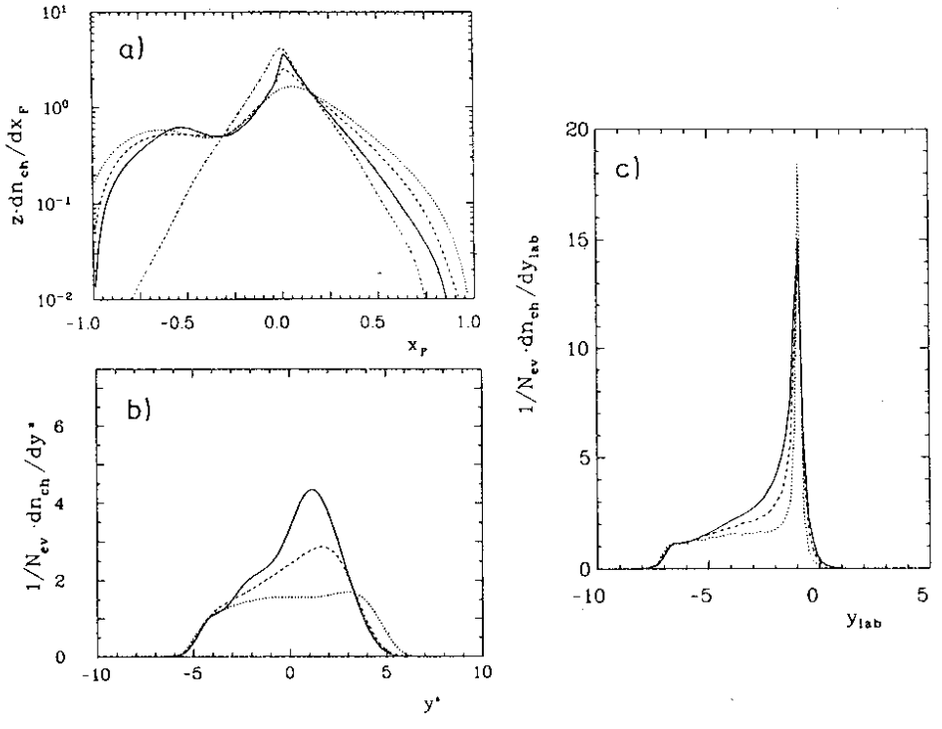

Figure 10: *Distribution of (a) energy-weighted scaled longitudinal momenta and (b) rapidity for charged particles in the hadronic CM frame of HERA events with $Q^2, W^2 > 10^3$ GeV^2 ($x_F > 0$ for the current jet and $x_F < 0$ for the target remnant jet). (c) Charged particle rapidity distribution in the lab frame for HERA events with $x = 0.1$, $y = 0.3$. Curves are for quark-parton model (dotted), first order QCD matrix elements (dashed), parton shower (full) and, in (a) only, e^+e^- events at the same energy (dash-dotted) [33].*

Studies of the hadronic final state is usually best performed in its CM frame where the separation of the current quark and the target remnant is much clearer than in the lab system where they can be close due to the strong boosts occuring in ep collider events. The longitudinal momentum distribution, Fig. 10a, for simulated HERA events [35] show the expected strong difference between the forward quark and backward target remnant hemispheres. The final state parton radiation from the struck quark makes the forward particles much softer than those originating from the non-radiating spectator remnant. This remnant, in the simplest case a diquark, produces a baryon which usually takes a larger energy fraction than a meson and thereby accentuate the forward-backward asymmetry [31]. These

effects give a rather different x_F-spectrum and lower multiplicity as compared to that obtained from a $q\bar{q}$ system produced in e^+e^- annihilation (at the same energy). The predominance of QCD radiation in the forward region is more clearly illustrated in the charged particle rapidity distribution, Fig. 10b. For the parton showers, this is partly related to the suppression of the initial state radiation due to the structure function constraints discussed in section 2. At fixed kinematical variables the current quark jet appears in the QPM model at a fixed lab rapidity resulting in a narrow peak in the charged particle rapidity distribution, shown in Fig. 10c which also illustrates the increasing jet width as first and higher order QCD effects are taken into account. By using less inclusive distributions it should be possible to make more detailed tests of QCD, e.g. based on the energy flow asymmetry, the energy-energy correlation and multijet events [33].

6 Jet characteristics at the TeV energy scale

Given that the jet models are based on sound physics input, i.e. are not just parametrizations of data, together with their ability to describe present-day jet data it becomes meaningful to make extrapolations to the much higher energy scale that will be available at future TeV colliders. There are also theoretical cross-checks that can be made to further increase the confidence in such extrapolations, e.g. by comparing Monte Carlo and analytical calculations in QCD [36]. Such a case is provided by the angular energy-energy correlation function [4], which is defined by

$$\frac{1}{\sigma}\frac{d\Sigma}{d\cos\theta} = \frac{1}{\sigma}\frac{1}{4}\sum_{A,B}\int_0^1 dx_A dx_B \frac{d\sigma(e^+e^- \to A+B+X)}{dx_A dx_B d\cos\theta}\cdot x_A x_B \qquad (13)$$

where the sum is over all particle pairs A, B with angle θ between $\vec{p}_A$ and the negative of $\vec{p}_B$. This function is shown in Fig. 11 for $e^+e^- \to q\bar{q}$ at an invariant mass of 3 TeV. The peak centered at the back-to-back direction $\theta = 0$ arise from two-jet final states in which one hadron is detected from each jet and the width of the peak is thus a measure of the angular width of a jet and is strongly affected by soft and collinear gluon emission. The two curves correspond to the analytical QCD calculation using two different approximations for the non-perturbative fragmentation, taken into account based on fits to present data. Since this calculation is based on quite different assumptions and approximations compared to the Monte Carlo, histograms in Fig. 11, it is reassuring to see the good agreement between the two approaches even when extrapolating to energies much higher than presently available, where they are both tuned to the data. It is also interesting to note that a parton shower algorithm without the coherence among soft gluons taken into account gives a different result compared to the coherent shower and the analytic calculation. This, and other considerations, make the incoherent cascade theoretically disfavoured, although such models can also be tuned to fit most aspects of current data which are, however, in a rather restricted energy region.

Although the bremsstrahlung nature of the QCD radiation predominantly results in soft and collinear parton emission, there will also be occasional hard emission at large angles resulting in the splitting of a jet into a sub-jet structure. Between these two extremes there is, of course, a continous distribution which makes the concept of a jet rather arbitrary from the theoretical point of view. The angular energy flow arising from a 1 TeV gluon jet

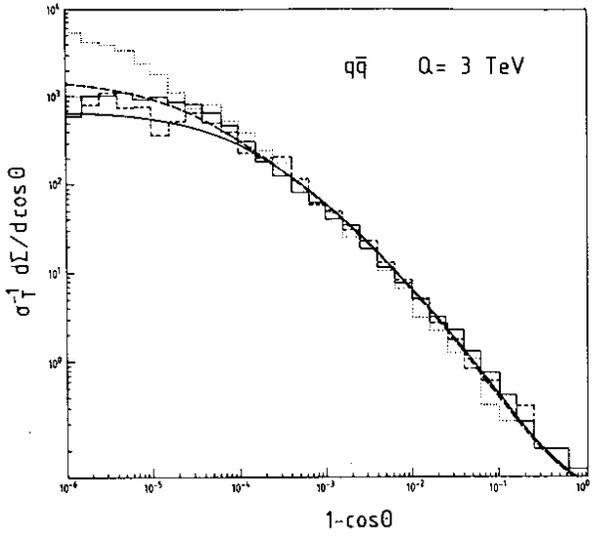

Figure 11: *The energy-energy correlation function, eq. (13), for a quark-antiquark system at $Q = 3$ TeV obtained from Monte Carlo simulation (histograms) of coherent parton shower evolution [6] with $t_{cut} = 0.5$ (full) and 5 GeV^2 (dashed), and without soft gluon interference ($t_{cut} = 5$ GeV^2, dotted) compared to analytical calculations (full and dashed curves) using two separate fits to data of non-perturbative effects [36].*

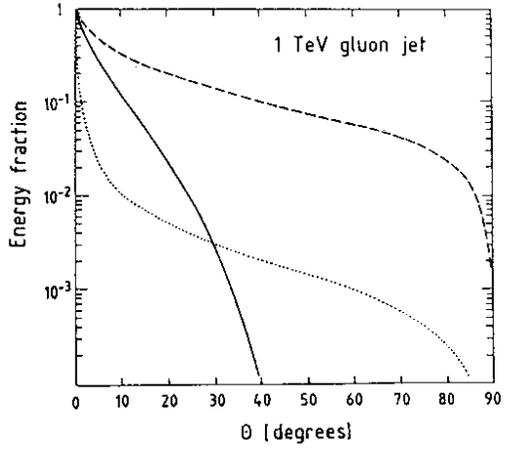

Figure 12: *Energy fraction outside a cone with half-opening angle θ, around the overall jet axis, i.e. parton direction, (dashed curve) and around the reconstructed (sub)jet axes (full curve) obtained from a gluon-gluon system with parton shower at $Q = 2$ TeV and, for comparison, without shower with θ relative to overall jet axis (dotted curve).*

is illustrated in Fig. 12. A very narrow jet is obtained with pure fragmentation, whereas a significant energy flow also at very large angles (with respect to the gluon direction) arise with the inclusion of parton radiation. The measured jet width will, however, be much smaller and depend on the resolution of sub-jet structures. This illustrates the importance of applying experimentally realistic jet definition criteria to the Monte Carlo generated events when predicting jet properties at TeV colliders. This can be done from the energy flow pattern, e.g., as follows. An idealized 'calorimeter' covers the full azimuthal angle around the beam axis and the pseudo-rapidity region $|\eta| \leq 3$ and is divided into cells of size $\Delta\eta \times \Delta\phi = 0.1 \times 5^0$ in each of which the particle energies of a Monte Carlo generated event are summed. Starting from the cell with largest transverse energy, $E_\perp$, the transverse energy of nearby cells within a cone of half-angle

$$\Delta R = \sqrt{\Delta\eta^2 + \Delta\phi^2} \leq 0.7 \qquad (14)$$

are summed. If $\sum E_\perp$ exceeds a certain cut-off value, E_c, then all the particles within the cone are said to form a jet with axis given by the $E_\perp$-weighted center of the cells. This procedure is iterated until all jets with $E_\perp$ larger than E_c, typically 10–20 GeV, are found. At TeV energies the details of this procedure make no difference. Thus, alternatives like using total energy rather than transverse energy or summing cell 4-vectors obtained from the energy deposited in and the location of the calorimeter cells, give essentially the same results. A coarser grained calorimeter, with cell size $\Delta\eta \times \Delta\phi = 0.2 \times 10^0$, also give similar results. The size of the cone used for the jet definition is, however, important for the jet properties since it regulates not only how many soft, wide angle particles that are included in the jet, but also the experimental resolution to separate nearby jets as indicated above.

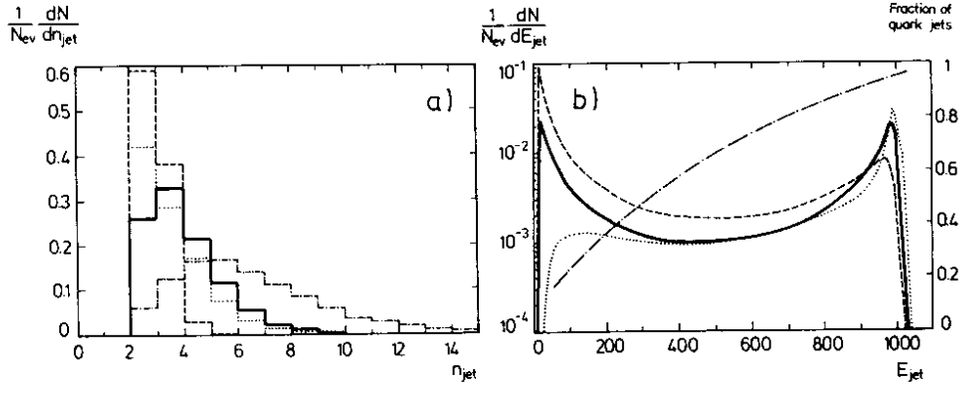

Figure 13: *(a) Number of reconstructed jets per e^+e^- event at 2 TeV. For the standard jet cone size $\Delta R = 0.7$: Coherent QCD cascade (full line), conventional cascade (dotted), 2^{nd} order matrix elements (dashed). For a smaller cone $\Delta R = 0.2$: coherent cascade (dash-dotted). (b) Energy distribution of reconstructed jets in e^+e^- at 2 TeV (left hand scale): Coherent QCD cascade (full curve), 2^{nd} order matrix elements (dotted), coherent cascade with $\Delta R = 0.2$ (dashed). Dash-dotted curve gives fraction of quark jets (right hand scale). From [37].*

A study [37] based on event simulation within the discussed framework [38] at a 2 TeV linear e^+e^- collider (discussed as a future possibility at CERN [39]) show the increase of the

jet multiplicity per event, Fig. 13a, as the higher order QCD effects in the parton shower is included, and also when the jet cone is decreased in size such that a finer sub-jet structure is resolved. As seen in the energy distribution of reconstructed jets, Fig. 13b, the additional jets arising in the parton shower model, compared to the $\mathcal{O}(\alpha_s^2)$ model, is mainly of lower energy and are predominantly gluon jets. Selecting only the higher energy jets produced at CM energies of 45, 100 and 2000 GeV (for details see [37]), the longitudinal and transverse energy flows within a jet are given in Fig. 14. The (relative) softening and narrowing of the jets with increasing energy is clearly seen. As an example for 1 TeV jets, 50% (10%) of the jet energy is carried by particles having fractional momentum $z > 0.08$ (0.3) corresponding to an absolute energy larger than 80 (300) GeV. The particle flow is furthermore less collimated than the energy flow, 50% of the *particles* in a jet are contained in a cone of half-angle of approximately 8^0, 6^0 and 3^0 for 45, 100 and 2000 GeV respectively, whereas 50% of the *energy* is within 6^0, 3^0 and 2^0 respectively.

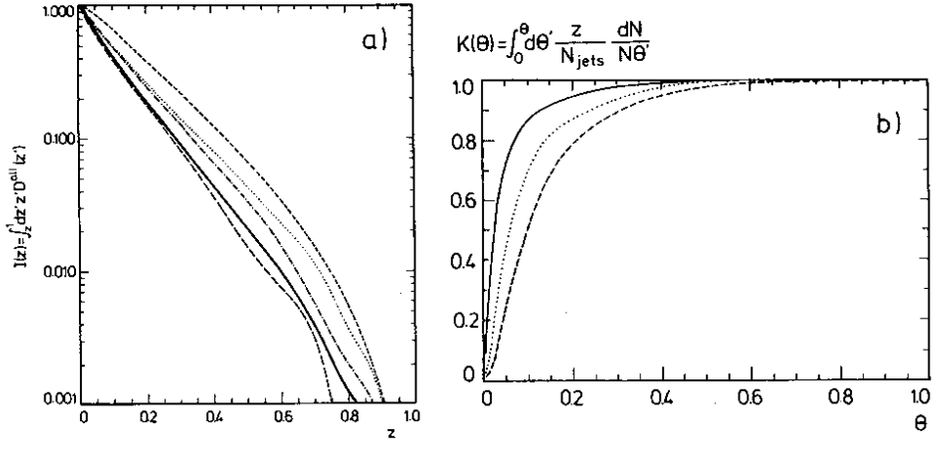

Figure 14: *(a) Integral of fragmentation function for all particles in 'high energy' jets (see (b)) in e^+e^- annihilation. At 2 TeV: Coherent QCD cascade (full curve), conventional cascade (dotted), coherent cascade with $\Delta R = 0.2$ (dash-dotted). Coherent QCD cascade with cluster hadronization [6] (long dashes). At 100 GeV: coherent cascade (dashed).*
(b) Integrated angular energy flow for all particles assigned to reconstructed 'high energy' jets, i.e. E_{jet} within [19,30], [45,55] and [900,1100] GeV in e^+e^- annihilation at cms energies of 45 (dashed curve), 100 (dotted) and 2000 GeV (full), respectively. Coherent parton cascade and string fragmentation in all cases. (Angle in radians.)

At a TeV hadron collider, like e.g. the LHC proposed at CERN [39], gluon jets will be abundantly produced. These are considerably softer than the quark jets, e.g. only 3.4% of the gluon jet energy is carried by particles having fractional momenta $z > 0.2$ whereas the corresponding number for quark jets is 23%. One should note that quark jets from a hadron collider are expected to have very similar properties as those from e^+e^- annihilation, since they are produced at comparable Q^2 scales. The soft fragmentation is independent of Q^2 and the perturbative scaling violations of the cascade vary as $\log Q^2$. The indicated results are

therefore more generally applicable. Furthermore, since the jet properties depend essentially only on the momentum transfer scale and not on the specific process producing them, jets originating from, e.g., the decay of some high mass state will have very similar properties. In fact, a significant part of the jet cross-section in 2 TeV e^+e^- collisons is due to W^+W^- production and decay into quark-antiquark pairs. Since the effective Q^2-scale for the gluon radiation from such quark jets is given by the W mass, these jets will have fragmentation properties similar to those at SLC/LEP (though boosted in the W-direction). The basic expectations of jet properties at the TeV energy scale should be rather clear from these examples and more details are not given here, but can be found in [37].

7 Conclusions

The importance of jet physics for understanding both perturbative and and non-perturbative aspects of QCD have been illustrated by discussing in some detail models for jet evolution in relation to existing experimental data and by indicating the energy dependence of the effects by extrapolation to future energy scales. The perturbative jet evolution models, taking higher order QCD into account by the parton shower approach, have reached a rather mature state including non-leading effects such as soft gluon coherence. The more phenomenological treatment of the non-perturbative hadronization has also developed into highly non-trivial models based of cluster formation or string formation and decay. It should be noted that these are not necessarily exclusive possibilities. A string can first decay into 'larger pieces', which can be identified with clusters, and then decay further into 'smaller pieces' or hadrons. In the Lund scheme, this is essentially equivalent to the chosen decay directly into hadrons. Cluster models, on the other hand, usually invoke a string-like longitudinal splitting of large mass clusters before the phase space decay is applied to cluster with mass below 3–4 GeV.

The complete jet simulation models formed from these physics input are capable of a rather precise description of present-day data, which thus serve to check the assumptions made and, furthermore, fix some crucial parameters. Considering also the theoretical constraints and cross-checks that are available, on can conclude that the extrapolation in order to predict jet properties in the TeV energy region can be viewed with rather much confidence. Of course, this extrapolation may turn out to fail when compared with reality. Even this should lead to an improved understanding since strictly speaking, as Bacon told us long ago, it is only possible to disprove a model by comparison with observation, although an agreement may justify some confidence. Smaller discrepancies may be cured by improving the models; large ones could be even more interesting since they would presumably indicate the occurrence of new physics phenomena!

References

[1] J. Ellis, M.K. Gaillard, G.G. Ross, Nucl. Phys. B111 (1976) 253
A. Ali et al., Nucl. Phys. B167 (1980) 454
K.J.F. Gaemers, J.A.M. Vermaseren, Z. Phys. C7 (1980) 81
R.K. Ellis, D.A. Ross, A.E. Terrano, Nucl. Phys. B178 (1981) 421

[2] R. Combridge, J. Kripfganz, J. Ranft, Phys. Lett. 70B (1977) 234
R. Cutter, D. Sivers, Phys. Rev. D16 (1977) 679; D17 (1978) 196
Z. Kunszt, E. Pietarinnen, Nucl. Phys. B164 (1980) 45, Phys. Lett. 132B (1983) 453
Z. Kunszt, W.J. Stirling, Phys. Lett. 171B (1986) 307 (and references therein).

[3] G. Altarelli, G. Martinelli, Phys. Lett. 76B (1978) 89
A. Méndez, Nucl. Phys. B145 (1978) 199
R. Peccei, R. Rückl, Nucl. Phys. B162 (1980) 125
Ch. Rumpf, G. Kramer, J. Willrodt, Z. Phys. C7 (1981) 337

[4] C. Basham, L. Brown, S. Ellis, S. Love, Phys. Rev. Lett. 41 (1978) 1585; Phys. Rev. D19 (1979) 2018; D24 (1981) 2382
Yu.L. Dokshitzer, D.I. D'yakonov, S.I. Troyan, Phys. Lett. 78B (1978) 290
J.C. Collins, D.E Soper, Nucl. Phys. B193 (1981) 381; B213 (1982) 545 (E); B197 (1982) 446

[5] G.C. Fox, S. Wolfram, Nucl. Phys. B168 (1980) 285
R.D. Field, S. Wolfram, Nucl. Phys. B213 (1983) 65
T.D. Gottschalk, Nucl. Phys. B214 (1983) and CALT-68-1083
R. Odorico, Nucl. Phys. B228 (1983) 381

[6] G. Marchesini, B.R. Webber, Nucl. Phys. B238 (1984) 1
B.R. Webber, Nucl. Phys. B238 (1984) 492

[7] M. Bengtsson, T. Sjöstrand, Nucl. Phys. B289 (1987) 810

[8] Yu.L. Dokshitzer, S.I. Troyan, Leningrad preprint LIYF 922

[9] G. Altarelli, G. Parisi, Nucl. Phys. B126 (1977)298
G. Altarelli, Phys. Rep. 81 (1982) 1

[10] T. Sjöstrand, Phys. Lett. 157B (1985) 321

[11] M. Bengtsson, T. Sjöstrand, M. van Zijl, Z. Phys. C32 (1986) 67

[12] R.D. Field, R.P. Feynman, Nucl. Phys. B136 (1978) 1

[13] G. Ingelman, Physica Scripta 33 (1986) 39

[14] D. Amati, G. Veneziano, Phys. Lett. 83B (1979) 87
A. Bassetto, M. Chiafoloni, G. Marchesini, Phys. Lett. 83B (1979) 207; Nucl. Phys. B163 (1980) 477

[15] C.-K. Ng, Phys. Rev. D31 (1985) 469

[16] B. Andersson, G. Gustafson, G. Ingelman, T. Sjöstrand, Phys. Rep. 97 (1983) 31

[17] T. Sjöstrand, Nucl. Phys. B248 (1984) 469

[18] T. Sjöstrand, Phys. Lett. 142B (1984) 420

[19] C. Peterson, Phys. Rev. D34 (1986) 1631

[20] B. Andersson, G. Gustafson, T. Sjöstrand, Phys. Scripta 32 (1985) 374

[21] B. Andersson, G. Gustafson, B. Söderberg, Z. Phys. C20 (1983) 317

[22] I. Montvay, Phys. Lett. 84B (1979) 331

[23] C. Peterson, T.F. Walsh, Phys. Lett. 91B (1980) 455

[24] A. Drescher, Thesis, Inst. f. Physik der Universität Dortmund, January 1987
U. Matthiesen, Thesis, Inst. f. Physik der Universität Dortmund, January 1987

[25] W. Bartel et al., JADE collaboration, Z. Phys. C33 (1986) 23

[26] G. Arnison et al., UA1 collaboration, Nucl. Phys. B276 (1986) 253

[27] P. Ghez, G. Ingelman, Z. Phys. C33 (1987) 465

[28] T. Åkesson et al., AFS collaboration, Z. Phys. C30 (1986) 27

[29] G. Ingelman, 'Deep inelastic physics at HERA', these proceedings.

[30] G. Ingelman, T. Sjöstrand, LU TP 80-12
B. Andersson, G. Gustafson, G. Ingelman, T. Sjöstrand, Z. Physik C9 (1981) 233, ibid. C13 (1982) 361

[31] G. Ingelman, B. Andersson, G. Gustafson, T. Sjöstrand, Nucl. Phys. B206 (1982) 239

[32] EMC Collaboration, J. J. Aubert et al., Phys. Lett. 95B (1980) 306, ibid. 100B (1981) 433, M. Arneodo et al., Phys. Lett. 149B (1984) 415, ibid. 150B (1985) 458, CERN-EP/87-112 (1987)

[33] M. Bengtsson, G. Ingelman, T. Sjöstrand, DESY 87-097

[34] M. Bengtsson, T. Sjöstrand, LU TP 87-10 (1987)

[35] G. Ingelman, LEPTO version 5.2, DESY preprint in preparation

[36] G. Ingelman, D.E. Soper, Phys. Lett. 148B (1984) 171

[37] P.N. Burrows, G. Ingelman, Z. Phys. C34 (1987) 91

[38] T. Sjöstrand, Computer Physics Communications 39 (1986) 347

[39] Proceedings of the workshop on Physics at Future Accelerators, La Thuile, Italy, January 1987, CERN 87-07